Ultrawideband Dispersion Control of a Metamaterial Surface for Perfectly-Matched-Layer-Like Absorption

Ultrawideband Dispersion Control of a Metamaterial Surface for Perfectly-Matched-Layer-Like Absorption

Dexin Ye,[1,2] Zhiyu Wang,[1,2] Kuiwen Xu,[1] Huan Li,[1] Jiangtao Huangfu,[1] Zheng Wang,[3] and Lixin Ran[1,*]

[1]*Laboratory of Applied Research on Electromagnetics (ARE), Zhejiang University, Hangzhou 310027, China*

[2]*Department of Physics, Massachusetts Institute of Technology, Cambridge, Massachusetts 02139, USA*

[3]*Department of Electrical and Computer Engineering, Microelectronics Research Center, the University of Texas at Austin, Texas 78758, USA*

(Received 13 January 2013; revised manuscript received 5 August 2013; published 29 October 2013)

Narrow bandwidth is a fundamental issue plaguing practical applications of metamaterial absorbers. In this Letter, we show that by deliberately controlling the dispersion and dissipation of a metamaterial, an ultrawideband perfect metamaterial absorber with complex-valued constitutive parameters strictly satisfying the modified model of a perfectly matched layer, can be achieved. The nearly perfect power absorption, better than 99%, was experimentally observed in an unprecedented bandwidth of 39%, approaching the theoretical Rozanov limit. We expect a wide range of applications to emerge from this general concept.

DOI: 10.1103/PhysRevLett.111.187402 PACS numbers: 78.68.+m, 41.20.−q, 78.20.Ci

Light propagation, focusing, and scattering are governed by the electromagnetic properties of the media being traversed [1]. These properties, either occurring naturally or synthesized with artificial metamaterials [2], must obey causality, which manifests as the Kramers-Kronig (K-K) relations between the real and imaginary parts of the frequency-dependent constitutive parameters, such as permittivity and permeability [3]. In natural media, dispersion and dissipation are determined by the underlying electronic and molecular energy levels, with largely limited tunability. In contrast, metamaterials are made of densely arranged subwavelength resonance cells, each scalable over decades of frequencies throughout microwave and optical regimes. The associated permittivity and permeability, either positive or negative, can be freely tuned over the entire range [4–6]. In the past decade, tremendous interest has risen in applying these unique dispersions toward novel applications, such as superlenses [7], invisibility cloaks [8], and perfect absorbers [9–18]. However, since these attractive applications rely on strong dispersions, they suffer from narrow bandwidth operation, which is a fundamental obstacle constraining metamaterials in practical applications.

In this Letter, we point out that a metamaterial can be created to have frequency-independent properties over an ultrawide frequency range, while maintaining its ability to exhibit electromagnetic characteristics that cannot be found in natural media. Based on the K-K relations, this can be achieved by combining multiple high-Q and low-Q resonances with deliberately controlled losses. To validate this approach, we experimentally demonstrated a metamaterial perfect absorber (MPA), whose frequency-independent dispersion regions of both permittivity and permeability are stretched to an ultrawide band, in which both the real and imaginary parts of the complex constitutive parameters are precisely tuned to satisfy a modified model of a perfectly matched layer (PML). Experimental data show that with a thickness of 0.2 free-space wavelength, such an MPA can achieve an unprecedented relative bandwidth of 39%, over which the power absorption remains over 99%. Analysis shows that the thickness of the MPA approaches the theoretical Rozanov limit, which provides the lower bound of the thickness of any physical absorber [19].

It is well-known that metamaterials exhibit Lorentzian dispersions, whose constitutive parameter $\chi(\omega)$, either the permittivity $\varepsilon(\omega)$ or the permeability $\mu(\omega)$, obeys the K-K relations [3–5]:

$$\mathrm{Re}(\chi(\omega)) = 1 + 2/\pi \int_0^{+\infty} d\omega' \,\mathrm{Im}(\chi(\omega'))\omega'/(\omega'^2 - \omega^2), \tag{1.1}$$

$$\mathrm{Im}(\chi(\omega)) = -2\omega/\pi \int_0^{+\infty} d\omega' [\mathrm{Re}(\chi(\omega')) - 1]/(\omega'^2 - \omega^2). \tag{1.2}$$

The K-K relations imply that the real part of a constitutive parameter can be tuned by controlling the imaginary part (or vice versa). Specifically, a metamaterial consisting of engineered subwavelength-scale cells makes it possible to modify dispersion by deliberately introducing multiple resonances with controlled dissipation. In what follows, we compare two analytical examples to illustrate how ultrawideband flat dispersions of constitutive parameters, where the real parts are either less than unity or negative, can be obtained by tuning three adjacent resonances. Subsequently, we show by full-wave simulations and experiments that an ultrawideband MPA with equal complex-valued constitutive parameters can be

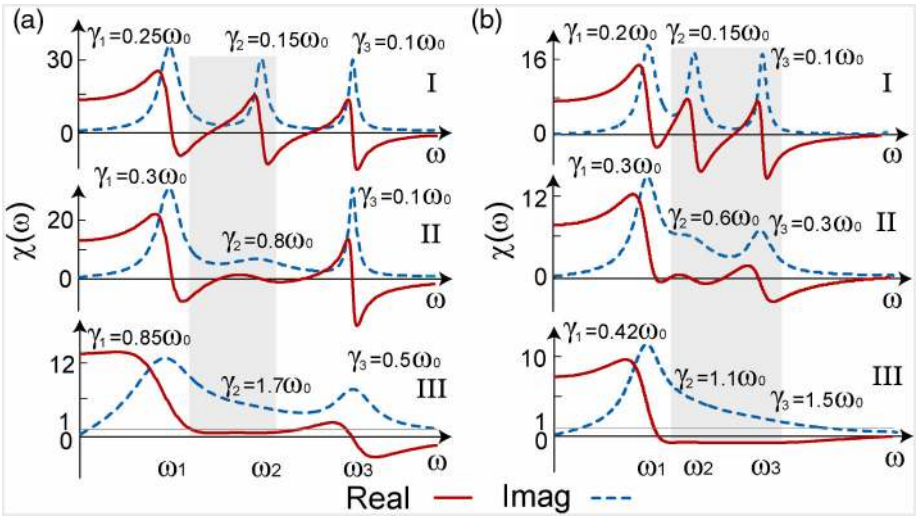

FIG. 1 (color online). Dispersion engineering of Lorentzian resonances to achieve a nearly constant positive value less than unity (a) and a negative value (b) within a wide target frequency range, where panels I, II, and III show the process of the dispersion control by varying the damping frequency.

implemented by introducing five electric and magnetic resonances in each unit cell.

A Lorentz model with three resonances can be expressed by

$$\chi(\omega) = 1 - \omega_{1p}^2/(\omega^2 - \omega_1^2 + i\omega\gamma_1) - \omega_{2p}^2/(\omega^2 - \omega_2^2 + i\omega\gamma_2) - \omega_{3p}^2/(\omega^2 - \omega_3^2 + i\omega\gamma_3), \quad (2)$$

where ω_i, ω_{ip} and, γ_i, are the resonance, plasma, and damping frequencies of the i-th resonance region ($i = 1$, 2, 3), respectively. Starting from $\omega_1 = \omega_0$, $\omega_2 = 2\omega_0$, $\omega_3 = 3\omega_0$, $\omega_{1p} = \omega_{2p} = \omega_{3p} = 3\omega_0$, and an initial set of damping frequencies of $\gamma_1 = 0.25\omega_0$, $\gamma_2 = 0.15\omega_0$, and $\gamma_3 = 0.1\omega_0$, $\chi(\omega)$, three resonance regions can be seen in panel I of Fig. 1(a). With small damping frequencies, the absorption exhibits a sharp dispersion spectrum near the resonance. In panel II, we see that after increasing the damping frequencies to $\gamma_1 = 0.3\omega_0$, $\gamma_2 = 0.8\omega_0$, and $\gamma_3 = 0.1\omega_0$, anomalous regions are spread out separately and the second dispersion region becomes flatter. Increasing the damping frequencies further to $\gamma_1 = 0.85\omega_0$, $\gamma_2 = 1.7\omega_0$, $\gamma_3 = 0.5\omega_0$, the real part of $\chi(\omega)$ is controlled to maintain a nearly constant positive value less than unity between ω_1 and ω_3, as shown in panel III. In the same way, we also control the damping frequencies to achieve a nearly constant negative real part of $\chi(\omega)$, as shown in Fig. 1(b). Assume $\omega_1 = \omega_0$, $\omega_2 = 1.48\omega_0$, $\omega_3 = 2.2\omega_0$, and $\omega_{1p} = \omega_{2p} = \omega_{3p} = 2\omega_0$, when γ_1, γ_2, and γ_3 are separately increased as indicated in panels I, II, and III, we can finally obtain a nearly constant, negative real part of $\chi(\omega)$. Note that in the shaded regions in Figs. 1(a) and 1(b), both relative bandwidths exceed 40%.

Recently, researches on new concept absorbers have attracted much attention [20–23]. Among them, MPAs show potential advantages in achieving nearly perfect absorption with subwavelength thickness [9–18]. Particularly, when an MPA's constitutive parameters are tuned to strictly satisfy a modified uniaxial PML model, the MPA maintains a nearly perfect absorption for normal and small-angle incidences [14]. Nevertheless, similar to other existing metamaterial applications, MPAs also suffer from limited bandwidths. To absorb energy in a thin layer without incurring any reflection, an MPA has to have large and equal imaginary parts of the permittivity and permeability, necessitating strong dispersions within the same band. Although engineering approaches can be used to combine multiple narrow band resonances [15–18], the overall absorption performances have not yet been comparable to PMLs. However, by making use of the dispersion control, we can realize a single-layer MPA with nearly perfect ultrawideband absorption. Such PML-like responses were previously only seen in theoretical studies with mathematically defined dispersions.

In order to obtain a perfect absorption over an ultrawide band, the complex permittivity and permeability tensors need to be identical over the specified band [14]. The identical tensors have a diagonal form diag(α, α, h), where h represents the permittivity and permeability component along the optical axis. To accomplish a nearly perfect absorption over a subwavelength material thickness, a large, positive imaginary part α'' for the complex-valued α ($\alpha = \alpha' + i\alpha''$) is required (See Supplemental Material [24]). For this purpose, we begin with the basic subwavelength unit cell consisting of metallic split-ring resonator (SRR) and rod, shown as "Cell 1" in Fig. 2(a) [25]. To introduce multiple electric and magnetic resonances without increasing the size of the cell, we split the original SRRs into four smaller, centrosymmetric SRRs, as illustrated by "Cell 2". To introduce independently tunable loss for each SRR, the outside corner of each SRR is cut

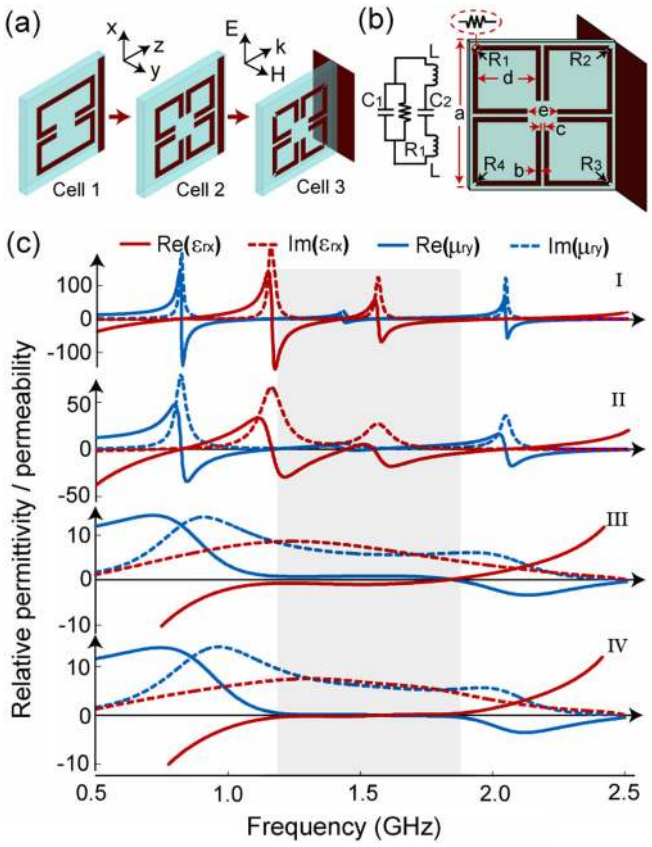

FIG. 2 (color online). Design of the unit cell of an ultrawideband MPA. (a) Introducing multiple resonances in an SRR and rod cell. (b) Topology of the new cell and related equivalent circuit model. (c) Retrieved constitutive parameters for different resistances.

and a lumped resistor is soldered, as shown by "Cell 3". Meanwhile, the rod is extended in the transverse plane to introduce a stronger electric resonance and provide a ground plane required by the uniaxial PML model [26,27].

The final topology of the new cell is shown in Fig. 2(b). For a y-polarized magnetic incidence, the equivalent circuit model for the top-left SRR is shown in the inset, where R_1 is the resistance introduced to tune the resonance, C_1 and C_2 are the capacitances of the gaps at the upper-left and lower-right corners, and L is the inductance determined by the length and width of the strips between the two gaps. By tuning the length, width of the strips, and especially, the intentionally introduced lumped resistance, one can tune both electric and magnetic resonances, and consequently, tune the real and imaginary parts of both permittivity and permeability tensors of the metamaterial.

To clearly show the effect of the dispersion control, we start by simulating an MPA consisting of the cells shown in Fig. 2(b). In each cell, four SRRs are printed on a 1.5 mm thick FR4 substrate with a dielectric constant of 4.4 and a loss tangent of 0.02. To ensure commercial surface-mount resistors exhibit negligible reactance, the dimensions of the unit cell are chosen to be $a = 40$ mm, $b = 1.2$ mm, $c = 0.4$ mm, $d = 16.4$ mm, and $e = 8$ mm, such that multiple resonances appear in a band centered at 1.5 GHz. Around this frequency, the periodicity of the unit cells is $\lambda/5$, and the MPA can be treated as an effective medium to retrieve effective constitutive parameters using a homogenization algorithm [28,29]. To retrieve the dispersions of the complex constitutive parameters from simulation data, we use a commercial Maxwell-equations solver, CST MWS, to perform full-wave simulations. Details of the parameter retrieval are provided in Supplemental Material [24].

In the process of controlling the dispersion, we first set the values of all four resistors to 1 Ohm, to obtain initial frequencies of the multiple resonance. In the panel I in Fig. 2(c), we find three magnetic resonances and two electric resonances in the band from 500 MHz to 2.5 GHz. Note that each resonance has a narrow bandwidth. After increasing the four resistances to 10 Ohm, we find in panel II that all the bandwidths of the resonances are broadened, in agreement with our theoretical analysis. When the four resistances are increased to 100 Ohm, we find in panel III that the second magnetic resonance and the two electric resonances inside the grey region become indistinguishable due to the increased dissipation, and both the imaginary and real parts inside the grey region become flatter. Finally, to achieve nearly perfect absorption in this band, the dispersions of both complex permittivity ε_r and permeability μ_r have to obey the modified PML model in the whole band, i.e., $\mathrm{Re}[\varepsilon_r] = \mathrm{Re}[\mu_r]$, $\mathrm{Im}[\varepsilon_r] = \mathrm{Im}[\mu_r]$, and $\mathrm{Im}[\varepsilon_r]$ and $\mathrm{Im}[\mu_r]$ should be larger than 2 (See Supplemental Material [24]). By performing a parameter sweep of the four resistances, we obtain an optimal set of 203, 122, 39, and 63 Ohms for resistors 1 to 4, respectively. With these values, the dispersions of the complex permittivity and permeability are nearly equal in the frequency band from 1.2 to 1.8 GHz, as shown in panel IV. In this band, the real parts of permittivity and permeability approach zero, while the imaginary parts are all larger than 5. Comparing with the absorption dependence with the thickness and imaginary parts shown in Fig. S1 in Supplemental Material [24], we achieve a nearly perfect ultrawideband absorption.

Based on the full-wave simulation, we show the effective wave impedance of the MPA layer and the greatly suppressed reflection coefficient $|S_{11}|$ at normal incidence [Figs. 3(a) and 3(b)]. The near-unity wave impedance of the MPA layer appears over the entire grey region (from 1.25 to 1.84 GHz), nearly the same as the impedance of air. The consequence is the lower than -30 dB reflection coefficient in the same region. Figure 3(c) plots the total power absorption inside the MPA layer and the power consumed by the resistors and other materials (i.e., substrate and the copper strips). We see that in the simulation, almost all the incident power is consumed by resistors, and the total power absorption is higher than 99.9% in a 0.59-GHz band from 1.25 to 1.84 GHz, corresponding to a relative bandwidth about 38% with respect to the central frequency. For the power absorption higher than 99%, the relative bandwidth increases to 50%. The lumped

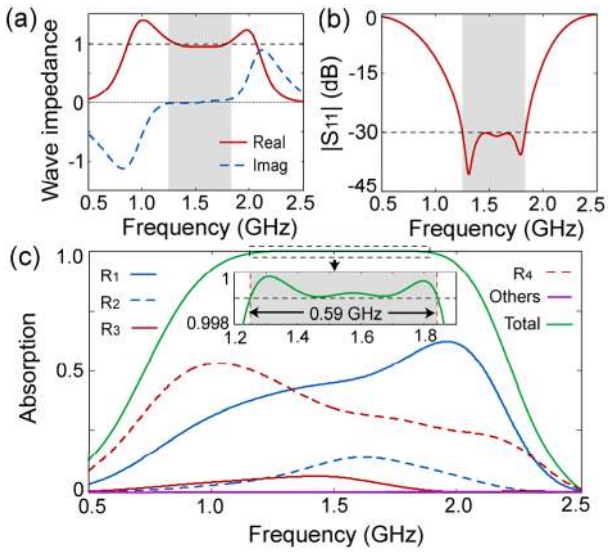

FIG. 3 (color online). Simulated wave impedance (a), reflection coefficient (b), and frequency-dependent power absorption for different resistors (c).

resistances play a key role in the precise dispersion control to achieve nearly perfect absorption.

To fabricate a polarization-independent MPA sample, the FR4 boards printed with the SRR units are cut and assembled into an interlocking lattice. The implemented 520×520 mm^2-sized sample includes 312 unit cells and 1248 surface-mount resistors, as shown in the inset of Fig. 4. Due to the cross coupling induced by the interlock, resistors R_1, R_2, R_3, and R_4 have been tuned to be 226, 324, 280, and 63.5 Ohms, respectively. The simulated absorption of the new MPA layer is given in Fig. 4. With these modified resistances, the 99.9% bandwidth of the power absorption is now 0.47 GHz (from 1.27 to 1.75 GHz), corresponding to a relative bandwidth of 31%.

We measure the power reflection and absorption of the MPA sample in a microwave anechoic chamber using an Agilent's 8722ES network analyzer and a pair of HD microwave's wideband horn antennas. For normal incidence, the reflection is measured with the MPA sample placed 1.5 meters away from the antenna, and the result is

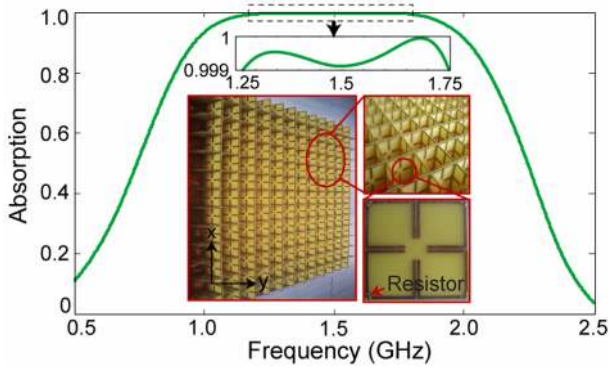

FIG. 4 (color online). Full-wave simulation of the fabricated MPA sample.

normalized with a control experiment using a copper board of an identical size. The center of the sample is carefully aligned with the center of the antenna aperture, as shown in the inset of Fig. 5(a). The normalized power absorption for both y- and x-polarized incidences are calculated by $1-|S_{11}|^2$, and are compared with simulation results in Fig. 5(a). We see that for the x-polarized incidence (blue line), the bandwidth in which the absorption is larger than 99% is 0.49 GHz (from 1.3 GHz to 1.79 GHz), corresponding to a relative bandwidth of 31.5%. For a y-polarized incidence (red line), the power absorption is similar to the x polarization.

Reflection at oblique incidence was then measured using two horn antennas as transmitter and receiver. The antennas were separated by an absorber screen to reduce mutual coupling, as shown in the inset of Fig. 5(a). The reflection from the MPA sample, as well as the copper board previously used in the control experiment, are separately measured as the incident angles change from 0° to 45°. Figure 5(b) plots the normalized power reflection versus incident angles. We see that in the cases when incident angles are smaller than 30°, the power absorption below −20 dB still occurs over an ultrawide bandwidth of 0.59 GHz (from 1.22 to 1.81 GHz), corresponding to a relative bandwidth of 39%.

For a physically realizable broadband nonmagnetic absorber, the Rozanov limit indicates that for any metal backed absorber under a normal incidence, its total thickness d must be larger than a theoretical limit for the given frequency response of the absorption [19], i.e.,

$$\left| \int_0^\infty \ln|R(\lambda)| d\lambda \right| \leq 2\pi^2 \mathrm{d}, \tag{3}$$

where R is the reflection coefficient and λ is the free-space wavelength. Note that our absorber consists of

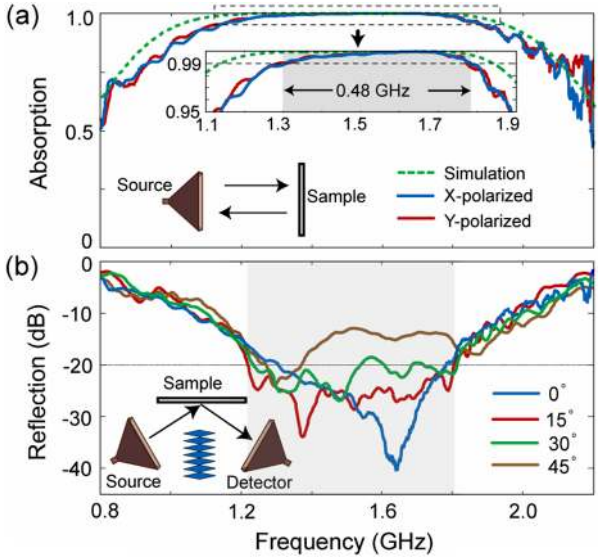

FIG. 5 (color online). Experimental absorption of the fabricated MPA sample. (a) Normal incidence. (b) Oblique incidences.

nonmagnetic copper wires and dielectric substrates, and therefore applies to Rozanov analysis. For the broadband absorption shown in Fig. 3(c), the corresponding theoretical limit is estimated to be 2.8 cm (given the data available, the integration is performed from 0.5 to 2.5 GHz). This value, likely underestimated, is close to the thickness (4 cm) of the designed MPA layer. For the measured data shown in Fig. 5(a), the calculated lower bound is about 2 cm, with the integration from 0.8 to 2.2 GHz. Although the MPA sample is slightly thicker than the underestimated lower bound, the $\lambda/5$-thick MPA sample is much thinner than pyramidal absorbers, which are typically thicker than 20 cm for the same operating band [30].

In conclusion, we show that the dispersions of the complex constitutive parameters of a metamaterial can be deliberately controlled to produce flat, ultrawide band frequency responses. In the example of implementing an ultrawideband MPA, we experimentally demonstrated highly precise dispersion control, capable of approximating a modified PML model requiring a strict, ultrawideband complex equality of the permittivity and permeability tensors. No such MPAs have been previously reported to accomplish this strict condition, nor has PML-like absorption been observed. It is worth noting that this approach also applies to achieving ultrawideband dissipation by controlling the real parts with tunable lumped reactance, to potentially obtain imaginary parts with novel frequency responses, such as mimicking a graphenelike conductivity in specified frequency ranges [31]. Based on the recent advancement of optical lumped nanocircuits [32,33], our approach may be extended to infrared and optical bands. We also expect several applications of this general principle of artificial dispersion control in the realization of various ultrawideband metamaterials.

This work is sponsored by the NSFC under Grants No. 61131002 and No. 61071063. Z. W. acknowledges support from the Alfred P. Sloan Research Fellowship.

*Corresponding author.
ranlx@zju.edu.cn

[1] L. D. Landau and *E. M. Lifshitz*, *The Classical Theory of Field* (Pergamon, New York, 1971).
[2] N. Engheta and R. W. Ziolkowski, *Electromagnetic Metamaterials: Physics and Engineering Explorations* (Wiley, New York, 2006).
[3] L. D. Landau and E. M. Lifshitz, *Electrodynamics of Continuous Media* (Pergamon, Oxford, 1984).
[4] J. B. Pendry, A. J. Holden, W. J. Stewart, and I. Youngs, Phys. Rev. Lett. **76**, 4773 (1996).
[5] J. B. Pendry, A. J. Holden, D. J. Robbins, and W. J. Stewart, IEEE Trans. Microwave Theory Tech. **47**, 2075 (1999).
[6] D. R. Smith, W. J. Padilla, D. C. Vier, S. C. Nemat-Nasser, and S. Schultz, Phys. Rev. Lett. **84**, 4184 (2000).
[7] J. B. Pendry, Phys. Rev. Lett. **85**, 3966 (2000).
[8] D. Schurig, J. J. Mock, B. J. Justice, S. A. Cummer, J. B. Pendry, A. F. Starr, and D. R. Smith, Science **314**, 977 (2006).
[9] N. I. Landy, S. Sajuyigbe, J. J. Mock, D. R. Smith, and W. J. Padilla, Phys. Rev. Lett. **100**, 207402 (2008).
[10] X. Liu, T. Starr, A. F. Starr, and W. J. Padilla, Phys. Rev. Lett. **104**, 207403 (2010).
[11] H. Tao, C. Bingham, A. Strikwerda, D. Pilon, D. Shrekenhamer, N. Landy, K. Fan, X. Zhang, W. Padilla, and R. Averitt, Phys. Rev. B **78**, 241103 (2008).
[12] N. Liu, M. Mesch, T. Weiss, M. Hentschel, and H. Giessen, Nano Lett. **10**, 2342 (2010).
[13] B. Wang, T. Koschny, and C. M. Soukoulis, Phys. Rev. B **80**, 033108 (2009).
[14] D. Ye, Z. Wang, Z. Wang, K. Xu, B. Zhang, J. Huangfu, C. Li, and L. Ran, IEEE Trans. Antennas Propag. **60**, 5164 (2012).
[15] H. Wakatsuchi, S. Greedy, C. Christopoulos, and J. Paul, Opt. Express **18**, 22 187 (2010).
[16] Y. Cui, J. Xu, K. H. Fung, Y. Jin, A. Kumar, S. He, and N. X. Fang, Appl. Phys. Lett. **99**, 253101 (2011).
[17] F. Ding, Y. Cui, X. Ge, Y. Jin, and S. He, Appl. Phys. Lett. **100**, 103506 (2012).
[18] Y. Cui, K. H. Fung, J. Xu, H. Ma, Y. Jin, S. He, and N. X. Fang, Nano Lett. **12**, 1443 (2012).
[19] K. N. Rozanov, IEEE Trans. Antennas Propag. **48**, 1230 (2000).
[20] Y. Huang *et al.*, Nat. Nanotechnol. **2**, 770 (2007).
[21] K. Mizuno, J. Ishii, H. Kishida, Y. Hayamizu, S. Yasuda, D. N. Futaba, M. Yumura, and K. Hata, Proc. Natl. Acad. Sci. U.S.A. **106**, 6044 (2009).
[22] M. A. Kats, D. Sharma, J. Lin, P. Genevet, R. Blanchard, Z. Yang, M. M. Qazilbash, D. N. Basov, S. Ramanathan, and F. Capasso, Appl. Phys. Lett. **101**, 221101 (2012).
[23] R. H. Yan, R. J. Simes, and L. A. Coldren, IEEE Photonics Technol. Lett. **1**, 273 (1989).
[24] See Supplemental Material at http://link.aps.org/supplemental/10.1103/PhysRevLett.111.187402 for a detailed process of retrieving parameters and numerical calculation on the absorption for the modified uniaxial PML.
[25] S. O'Brien and J. B. Pendry, J. Phys. Condens. Matter **14**, 4035 (2002).
[26] Z. S. Sacks, D. M. Kingsland, R. Lee, and J.-F. Lee, IEEE Trans. Antennas Propag. **43**, 1460 (1995).
[27] S. D. Gedney, IEEE Trans. Antennas Propag. **44**, 1630 (1996).
[28] X. Chen, T. M. Grzegorczyk, B.-I. Wu, J. Pacheco, and J. A. Kong, Phys. Rev. E **70**, 016608 (2004).
[29] D. R. Smith, S. Schultz, P. Markos, and C. M. Soukoulis, Phys. Rev. B **65**, 195104 (2002).
[30] B. T. Dewitt and W. D. Burnside, IEEE Trans. Antennas Propag. **36**, 971 (1988).
[31] T. Stauber, N. M. R. Peres, and A. K. Geim, Phys. Rev. B **78**, 085432 (2008).
[32] Y. Sun, B. Edwards, A. Alu, and N. Engheta, Nat. Mater. **11**, 208 (2012).
[33] N. Liu, F. Wen, Y. Zhao, Y. Wang, P. Nordlander, N. J. Halas, and A. Alù, Nano Lett. **13**, 142 (2013).